IEEJ Journal of Industry Applications
Vol.7 No.1 pp.64–72 DOI: 10.1541/ieejjia.7.64

Paper

Design Optimization of Primary Core in Induction Heating Roll by the Combination of 2D Level-set Method and 3D Coupled Magnetic-Thermal FEM

Kazuki Hirono[*a)] Student Member, Reona Hoshino[*] Student Member
Tsuyoshi Kamiya[*] Student Member, Shinji Wakao[*] Member
Yoshifumi Okamoto[**] Senior Member, Woojin Jeon[***] Non-member

(Manuscript received March 23, 2017, revised Aug. 10, 2017)

We present a novel practical design optimization for the primary core in an induction heating roll, which significantly affects the heating performance. To optimize the 3D eddy current field problem within an acceptable CPU time, we effectively combine 2D magnetostatic optimization and 3D coupled magnetic-thermal FEM. For the 2D optimization, we adopt the level-set method, which has an advantage of being able to derive a feasible shape. However, the disadvantage is that its result occasionally falls into a local optimal solution. To overcome this disadvantage, we propose conducting the initial conceptual design with the linear level-set method before using the nonlinear level-set method to expand the search domain. Furthermore, we incorporate the parallelized move-limit strategy into the level-set method to prevent the configuration from undergoing excess deformation by the operation for the area constraint. Finally, the 2D optimal shape obtained using our new level-set method is converted into a straight line cross-sectional configuration to improve manufacturability, and the final 3D design is created with slits. The final 3D design obtained as a result of the 3D FEM successfully improves both the heating speed and temperature uniformity on the surface of the heating part under the same conditions of input AC current and material volume.

Keywords: coupled magnetic-thermal analysis, design optimization, finite element method, induction heating, level-set method, move-limit

1. Introduction

Heating rolls are applicable to various kinds of manufacturing process in textile, non-woven, paper, printing and film industries. Recently, induction heating is becoming wide spread for generating heat because of its fast response to input changes which allows easy output controls. Through multiple means, induction heating machinery has been enhanced as follows: By inserting heat pipes with very high thermal conductivity, uniformity of the outer surface temperature of the roll is improved [(1)]. The amplitude and frequency of the current and the coil position and volume are optimized to ameliorate the heating efficiency [(2)(3)]. In addition, primary core design is also important because it determines the magnetic flux distribution in the secondary core which has a great influence on the heating performance. However, there are few reports on the primary core design.

a) Correspondence to: Kazuki Hirono. E-mail: hsvvjsm@akane.waseda.jp
* Department of Electrical Engineering and Bioscience, Waseda University
3-4-1, Okubo, Shinjuku-ku, Tokyo 169-8555, Japan
** Department of Electrical and Electronic Engineering, Hosei University
3-7-2, Kajinocho, Koganei, Tokyo 184-8584, Japan
*** Dongwonroll Co., Ltd.
374-12, Samsan-dong, Incheon 409-090, Korea

Since conceptual design is semi-automatically derived, optimization methods are often utilized for electrical equipment design. Topology optimization has a potential for reaching higher performance solution in comparison with other optimization because it allows the changes in topology as well as the shape of target structure. However, topology optimization occasionally falls into an unfeasible solution. Among a variety of topology optimization methods, level-set method [(4)–(6)] is an attractive design tool because this method can obtain a more practical shape. Although this method is expected to be applied to the design of many actual devices, its current use, as far as we know, is limited to only IPM motor [(6)] in a magnetic analysis.

In this paper, we focus on the 3D design optimization of a primary core in an induction heating roll by level-set method. The purpose of this optimization is to improve heating speed and temperature uniformity on the surface of the heating part. Since this 3D design optimization problem takes an unacceptably long CPU time, we positively approximate this problem by appropriately considering physical phenomenon in the roll. We propose the combination of 2D magnetostatic level-set method and 3D coupled magnetic-thermal FEM. First, we define 2D magnetostatic optimization model in consideration of physical phenomenon. Second, we carry out 2D shape optimization of the primary core by level-set method with magnetic nonlinearity. Before the nonlinear level-set

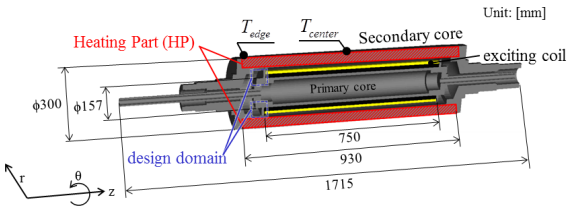

Fig. 1. 3D structure of an induction heating roll (half region)

method (NL-LS), we propose an ingenious approach with the initial conceptual design by linear level-set method (L-LS), i.e., we adopt the optimal shape by L-LS as the initial shape of NL-LS. Furthermore, we suggest the parallelized move-limit strategy which selects the best time step size in level-set method. It enables us to avoid over-correction of the level-set function and consequently obtain a more feasible shape. Finally, we convert the 2D optimal shape produced by our new level-set method into a straight line cross-sectional configuration to facilitate the manufacture. In creating 3D design by rotating the cross-section, we arrange slit structure which aims to save weight while maintaining performance. To demonstrate the validity of our proposed design optimization method, the 3D design is evaluated by the 3D coupled magnetic-thermal FEM which considers magnetic nonlinearity properties. As a result, the final 3D design successfully improves both heating speed and temperature uniformity on the surface of the heating part under the same conditions of input AC current and material volume.

2. Heating Principle of Induction Heating Roll

Figure 1 shows the half of the structure of an induction heating roll. The primary core is composed of silicon, carbon, stainless steel and the secondary core consists of carbon steel. Alternating flux generated by the exciting coil flows from the primary core to the secondary core. Then the magnetic flux induces an eddy current in the carbon steel in the secondary core, which heats the roll. Therefore, primary core has a significant influence on the heating performance because primary core decides the magnetic flux distribution in the secondary core which induces an eddy current. Especially, we focus on the design of primary core tip located between primary and secondary cores, which affects how magnetic flux flows from primary core to secondary core. In order to maximize the performance, we conduct the topology optimization of tip which has higher freedom than that of other optimization, such as size and shape optimization. Since topology optimization tends to reach an unfeasible solution, we adopt level-set method which enables us to improve the feasibility of solution in comparison with other topology optimization methods.

3. Design Optimization Methods

3.1 Combination of 2D Level-set Method and 3D Coupled Magnetic Thermal FEM In this paper, we perform 3D design optimization of the primary core in an effort to improve the heating performance. Since this 3D eddy current field optimization problem takes an unacceptably long CPU time, we combine 2D magnetostatic level-set method and 3D coupled magnetic-thermal FEM to reduce the computational

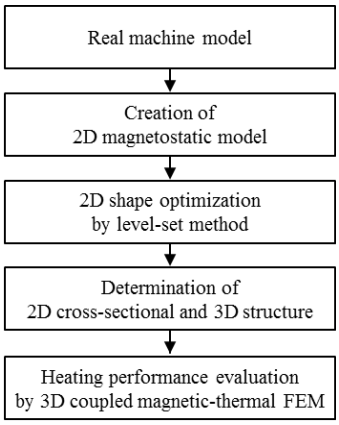

Fig. 2. Flowchart of the proposed design optimization method

cost positively. The flowchart of this combined design optimization method is shown in Fig. 2. First, we simplify the real machine model into the 2D magnetostatic optimization model in consideration with the characteristics of physical phenomenon. Since the distribution of eddy currents greatly depends on that of magnetic flux flow, we convert the eddy current field problem into the magnetostatic field one. Furthermore, we can appropriately approximate the flux distribution in the 3D model into that in the 2D one in consideration with the symmetry of the investigated roll. Therefore, we convert the 3D model into 2D one as shown in Fig. 2, which enables us to dramatically reduce the computational burden. Second, we implement level-set method with magnetic nonlinearity to derive the conceptual design indicating the optimal magnetic circuit. Third, the obtained conceptual design is converted into a straight line cross-sectional configuration to improve manufacturability while keeping the magnetic circuit. Finally, we create the final 3D design with slits by rotating the cross-section. The final 3D design with slits is evaluated by the 3D coupled magnetic-thermal FEM with magnetic nonlinearity and we confirm the validity of the proposed design optimization method. The theory of each method is detailed in the following sections in this chapter.

3.2 Level-set Method For the optimization, we adopt a level-set method which is an attractive design tool for real machines. In this method, material boundaries are represented by the zero-isosurfaces of the level-set function. The optimization is progressed with the advection on the basis of the design sensitivity. The advantage of this method is the feasibility of the optimal shape because the grayscale width is restricted to the vicinity of the material boundary. The drawback is that its result is sometimes trapped by a local optimal solution. The detailed formulation of the level-set method is shown in the following subsections.

3.2.1 Representation of the Material Boundaries

The level-set function is defined as the signed distance function $\phi(x)$ described in (1). The function represents a material boundary between a magnetic body and air as shown in Fig. 3(a).

$$\phi(x) = \begin{cases} d(x, \partial\Omega) & (x \in \Omega) \\ 0 & (x \in \partial\Omega) \\ -d(x, \partial\Omega) & (x \notin \Omega) \end{cases} \cdots\cdots\cdots\cdots\cdots\cdots (1)$$

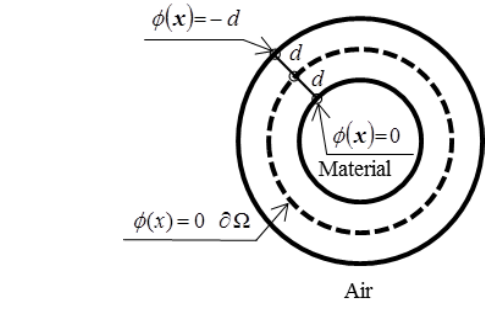

(a) level-set function

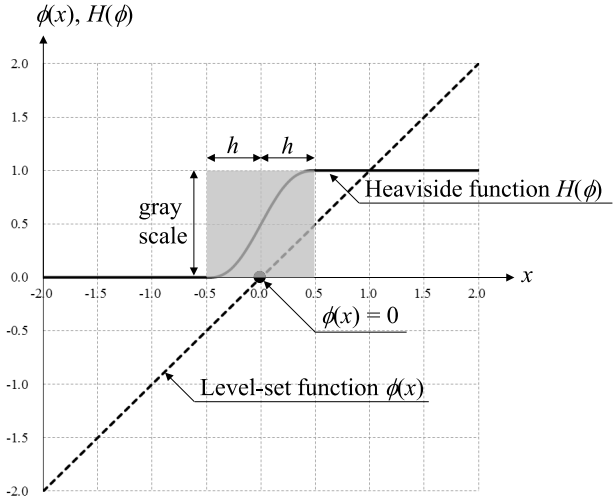

(b) Heaviside function

Fig. 3. Shape description by level-set method

where Ω, $\partial\Omega$, and $d(x, \partial\Omega)$ are the material region, the material boundary between the magnetic body and air, and the shortest distance from the material boundary respectively.

Next, we assign the level-set function $\phi(x)$ to the Heaviside function $H(\phi)$ formulated in (2) for continuously expressing the material density information from 0 to 1 as shown in Fig. 3(b).

$$H(\phi)=\begin{cases}0 & (\phi<-h)\\ \dfrac{1}{2}+\dfrac{15}{16}\left(\dfrac{\phi}{h}\right)-\dfrac{5}{8}\left(\dfrac{\phi}{h}\right)^3+\dfrac{3}{16}\left(\dfrac{\phi}{h}\right)^5 & (-h\le\phi<h)\\ 1 & (h\le\phi)\end{cases} \cdots\cdots (2)$$

where h is the transition width between the magnetic body and air, which also means the gray scale range.

The magnetic reluctivity of each element in the design domain is formulated as follows:

$$\nu(\phi, \boldsymbol{B}^2)=\nu_0+(\nu_e(\boldsymbol{B}^2)-\nu_0)H(\phi) \cdots\cdots (3)$$

where ν_0 and $\nu_e(\boldsymbol{B}^2)$ are the magnetic reluctivity in a vacuum and in a magnetic body respectively.

3.2.2 Advection of the Material Boundaries

Material boundaries satisfy (4) at an arbitrary time.

$$\phi(\boldsymbol{x}, t)=0 \cdots\cdots (4)$$

Here, we differentiate (4) with respect to time t as follows:

$$\frac{\partial\phi(\boldsymbol{x}, t)}{\partial t}+|\nabla\phi|\, v_n=0 \cdots\cdots (5)$$

where v_n is the normal component of the velocity vector.

Since the level-set function has the characteristic of the signed distance, $|\nabla\phi|=1$ is satisfied. Thus, (5) can be rewritten as (6). Although $|\nabla\phi|=1$ becomes unsatisfied after updating the level-set function, this problem is avoidable by applying a regularization technique [5].

$$\frac{\partial\phi(\boldsymbol{x}, t)}{\partial t}+v_n=0 \cdots\cdots (6)$$

The update of level-set function is formulated with forward Euler time integration as follows:

$$\boldsymbol{\Phi}^{(k+1)}=\boldsymbol{\Phi}^{(k)}+\Delta t\boldsymbol{V}_{\boldsymbol{H}}^{(k)} \cdots\cdots (7)$$

where k is the number of the iteration, $\boldsymbol{\Phi}$ is the level-set function vector, Δt is the time step size, and $\boldsymbol{V}_H$ is the velocity vector. $\boldsymbol{V}_H$ is calculated by the following equation;

$$A_H\boldsymbol{V_H}^{(k)}=\boldsymbol{b_H}^{(k)} \cdots\cdots (8)$$

where A_H and $\boldsymbol{b_H}^{(k)}$ are given as follows:

$$A_H|_{i,j}=\int_{\Omega_d}N_iN_jdV \cdots\cdots (9)$$

$$\boldsymbol{b_H}^{(k)}|_i=-\int_{\Omega_d}N_i\nu_n^{(k)}dV \cdots\cdots (10)$$

where N_i is the nodal interpolation function and Ω_d is the design domain. Here, we assign the node-based design sensitivity $\partial W/\partial\phi$ to v_n. The calculation of $\partial W/\partial\phi$ is described in 3.2.3.

In respect to time step size Δt in (7), Δt is restricted by Courant-Friedrichs-Lewy (CFL) condition for numerical stability shown in (11).

$$\Delta t\le\frac{\Delta x_{\min}}{\left\|\boldsymbol{V_H}^{(k)}\right\|_\infty} \cdots\cdots (11)$$

where $\Delta x_{\min}$ is the minimum edge of elements in the design domain and $\|\boldsymbol{V_H}^{(k)}\|_\infty$ is the maximum value of the velocity vector.

3.2.3 Sensitivity Analysis using Adjoint Variable Method (AVM) The design sensitivity $\partial W/\partial\phi$ assigned to the velocity vector v_n is calculated with adjoint variable method (AVM). AVM enables us to derive the design sensitivity in one calculation. The linear equation of an adjoint problem without constraints is given as follows:

$$\frac{\partial W}{\partial\phi_i}=\boldsymbol{\lambda}^T\left[\left.\frac{\partial K}{\partial\phi_i}\right|_n \mathrm{A}_n\right]$$

$$\left(K+\left.\frac{\partial K}{\partial A}\right|_n A_n\right)^T\boldsymbol{\lambda}=\left.\frac{\partial W}{\partial A}\right|_n \cdots\cdots (12)$$

where K is the stiffness matrix, $\boldsymbol{A}$ is the magnetic vector potential, ϕ_i is the level-set function at the i-th node, and $\boldsymbol{\lambda}$ is the adjoint variable.

3.2.4 Considering Area Constraint In general, an area constraint condition is formulated as follows:

$$G(\phi)=S(\phi)-S_0\le 0 \quad \left(S(\phi)\equiv\int_{\Omega_d}H(\phi)dS\right) \cdots\cdots (13)$$

If (13) is not satisfied after updating the level-set function,

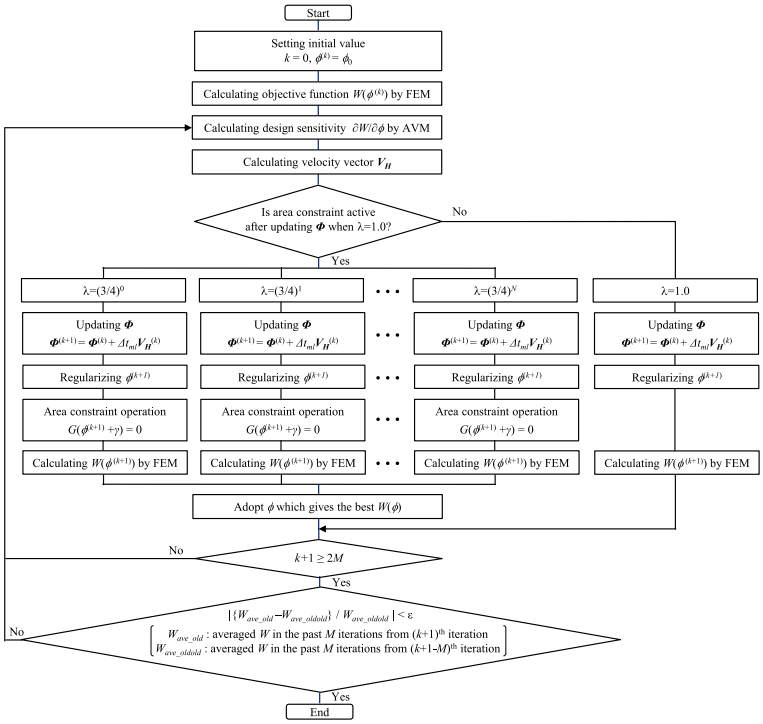

Fig. 4. Flowchart of the level-set method with the move-limit strategy

we correct level-set function by solving (14) with regard to $\gamma^{(5)}$.

$$G(\phi^{(k+1)}+\gamma)=0 \cdots\cdots (14)$$

This operation indicates equally lowering the level-set function values while maintaining the configuration. In 3D analysis, the same procedure is able to be employed as a volume constraint. The merit is easy convertibility to a problem without constraints, thus we can use (12). However, on occasion this operation can greatly deform the configuration. To prevent this unfavorable deformation, we incorporate the move limit strategy into the level-set method detailed in the next subsection.

3.2.5 Proposal of Move-limit Strategy For a time step size Δt in a level-set method, the upper value of the CFL condition, i.e., $\Delta t = \Delta x_{\min}/\|V_H{}^{(k)}\|_\infty$ is often adopted in a magnetic analysis. However, in this case, an unfavorable deformation can occur because the correction width by the area constraint operation might be too big depending on the problem. In structural optimization, move limit strategy is extensively used and is also applied to a level-set method [7], but there are some additional parameter settings to consider. Hence, we propose a novel parallelizable move-limit strategy. Time step size calculated by our proposed move-limit strategy Δt_{ml} is formulated as follows:

$$\Delta t_{ml}=\lambda_{best}\cdot\frac{\Delta x_{\min}}{\left\|\boldsymbol{V_H}^{(k)}\right\|_\infty} \cdots\cdots (15)$$

where λ_{best} is the best move-limit coefficient which is selected as described in the following explanations.

As for move-limit coefficients λ, multiple values from 0 to 1 are set. In this paper, for instance, λ is formulated as (16).

$$\lambda=\left(\frac{3}{4}\right)^i \cdots\cdots (16)$$

where i ranges 0 to N. $N+1$ is the number of parallelization and is set to 33 in this paper.

The best move-limit coefficient λ_{best} is chosen in accordance with the flowchart of the level-set method with the move-limit strategy as shown in Fig. 4. When area constraint is active, the move-limit scheme is started. Using various λ given in (16), we parallely update level-set function with reguralization and conduct area constraint operation. Then the best move-limit coefficient λ_{best} is selected, which gives the best objective function. This is iterated until the convergence condition is satisfied. Here, M and ε are adopted 10 and 10^{-6} in the convergence condition in Fig. 4. The proposed move-limit strategy is easily implementable and takes the same time as the conventional level-set method because of the parallelization.

3.3 Magnetic Field Analysis with Eddy Current In magnetic analysis, we adopt A-ϕ method considering nonlinear magnetization properties of the carbon and the silicon steel. The governing equations are as follows:

$$\mathrm{rot}(\nu\,\mathrm{rot}\,\boldsymbol{A})=\boldsymbol{J_0}+\boldsymbol{J_e} \cdots\cdots (17)$$

$$\boldsymbol{J_e}=-\sigma\left(\frac{\partial \boldsymbol{A}}{\partial t}+\mathrm{grad}\,\phi\right) \cdots\cdots (18)$$

$$\mathrm{div}\boldsymbol{J_e}=0 \cdots\cdots (19)$$

where $\boldsymbol{A}$ is the magnetic vector potential, $\boldsymbol{J}_0$ is the source current density, ϕ is the electric scalar potential, ν is the magnetic reluctivity, and σ is the electrical conductivity.

It is necessary to use backward difference approximation with respect to $\partial\boldsymbol{A}/\partial t$ in (18) because $\boldsymbol{A}$ is a distorted wave in a nonlinear field. The analysis is continued until the eddy current reaches the steady state. Here, for the purpose of deriving the steady state quickly, we also calculate the nonlinear complex equation using phasor notation by complex Newton-Raphson method with the help of Wirtnger calculus [8] and let

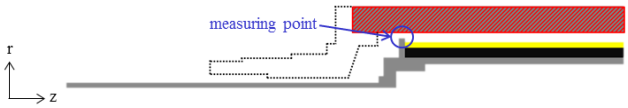

Fig. 5. Cross-sectional structure of an induction heating roll for measuring magnetic flux density (1/4 region)

Table 1. Comparison between computational and measured magnetic flux densities

	Measured	Computational	Relative error
B [G]	776	799	2.96 %

the results be the initial value of $\boldsymbol{A}$.

To confirm the validity of the magnetic analysis, we conduct a measurement of the magnetic flux density with the experimental roll detached edge of the secondary core, as depicted in Fig. 5. Table 1 shows the comparison between the computational results and the measured data and demonstrates the validity of the magnetic analysis.

3.4 Coupling Thermal Analysis We perform one-way coupling thermal analysis with magnetic analysis to obtain the transient temperature distribution which indicates heating performance. The governing equation of the thermal analysis is given by (20).

$$\mathrm{div}\,(\lambda\,\mathrm{grad}\,T) + Q = \rho c\frac{\partial T}{\partial t} \cdots\cdots (20)$$

where T is the temperature, Q is the heat source, λ is the thermal conductivity, ρ is the material density, c is the material specific heat.

Here, the thermal analysis is linear, thus we do not consider temperature dependent properties of the materials in the induction heating roll. The thermal analysis is carried out with the previously obtained eddy current in the magnetic analysis. We set the averaged value of the eddy current loss density in a cycle in a steady state, as the heat source input as calculated in (21) because thermal conduction phenomenon are much slower than magnetic phenomenon.

$$Q = \frac{1}{\tau}\int_{t}^{t+\tau}\frac{|\boldsymbol{J_e}|^2}{\sigma}dt \cdots\cdots (21)$$

where τ is the cycle time of eddy current wave.

We set the boundary condition (22) on the surface between air and the outermost part of the roll.

$$q = \alpha(T - T_f) \cdots\cdots (22)$$

where α is the heat transfer coefficient, T is the temperature on the boundary surface, and T_f is the temperature of the air.

To determine the heat transfer coefficient α, we measure transient temperature at the center of the heating part of the roll in Fig. 1 at each 10 minute time interval when the roll is heated for 90 minutes. As a result, we let α be 14 W/(m$^2\cdot$°C) which provides the best fit to the measured data as shown in Fig. 6. The comparison between the computational results and the measured data in the case of α = 14 W/(m$^2\cdot$°C) is shown in Fig. 7. Figure 6 and Fig. 7 demonstrate the validity of the thermal analysis.

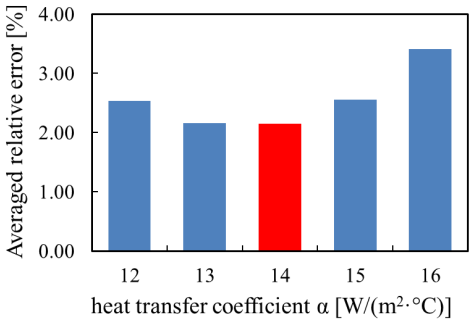

Fig. 6. Averaged relative errors between computational and measured surface temperature at the center of the heating part with various heat transfer coefficient α

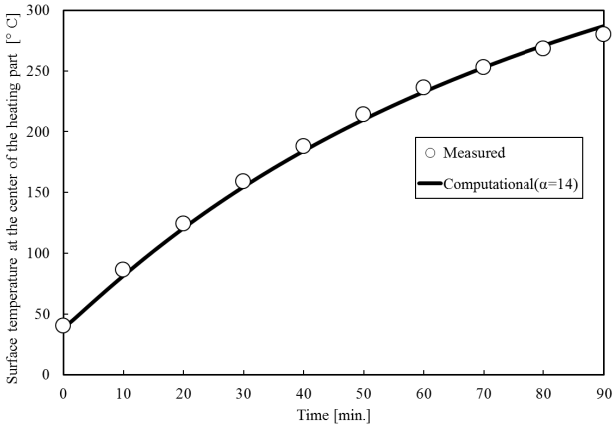

Fig. 7. Transient surface temperature at the center of the heating part in the case of α = 14

4. Design Optimization of Primary Core in Induction Heating Roll

4.1 2D Optimization Model for Level-set Method

We define the 2D magnetostatic model for level-set method as shown in Fig. 8. The design domain is located in the primary core tip which most impacts the magnetic flux distribution in the secondary core. The topology optimization aims to derive the optimal structure of silicon steel in the design domain. The purpose of the design optimization is to improve heating speed and temperature uniformity in an eddy current field. In the magnetostatic optimization model, we define the objective function as the magnetic energy stored in the edge of the heating part (target area Ω_t) as described in (23) for the following reasons: The magnetic flux passing through Ω_t flows through the whole heating part and induces eddy current. The increase in the value of the objective function is expected to improve the heating speed and the temperature uniformity simultaneously.

$$\max.\quad W = \int_{\Omega_t}\frac{1}{2}\nu B^2 dS \cdots\cdots (23)$$

In addition, the area constraint condition (24) is built so that the area of Ω_{opt} does not become larger than that of the current shape Ω_c.

$$\text{s.t.}\quad G = S_{\Omega opt} - S_{\Omega c} \le 0 \cdots\cdots (24)$$

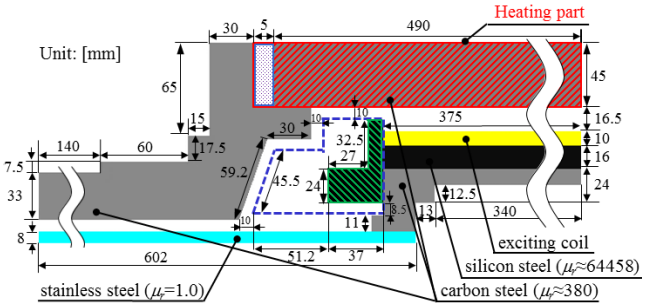

(a) Overall view

μ_r is the relative magnetic permeability in linear analysis. In nonlinear analysis, magnetic nonlinear properties of silicon steel and carbon steel are considered

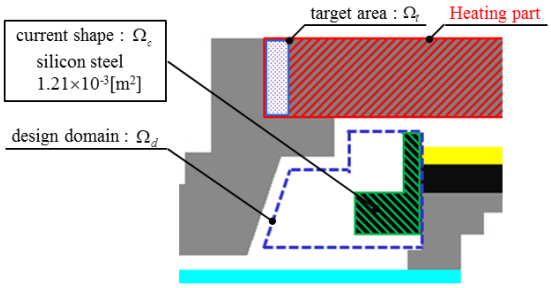

(b) Enlarged view

Fig. 8. 2D optimization model for level-set method

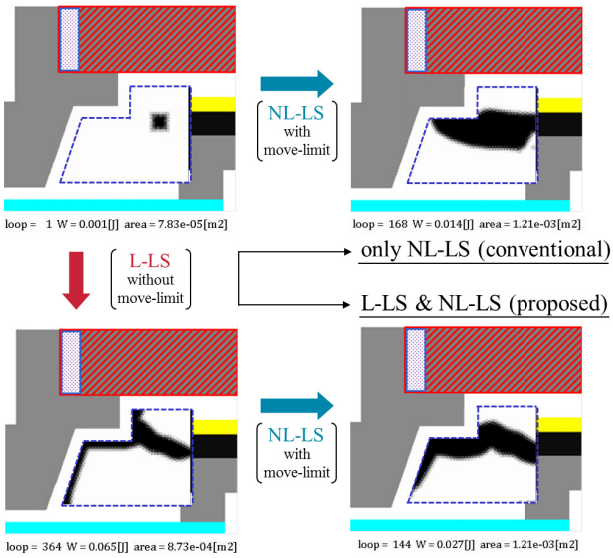

Loop, W, and area in the figure are the iteration number, the objective function value, and the area of the shape respectively.

Fig. 9. Optimization results by only NL-LS and combined L-LS & NL-LS, with an initial shape of a square

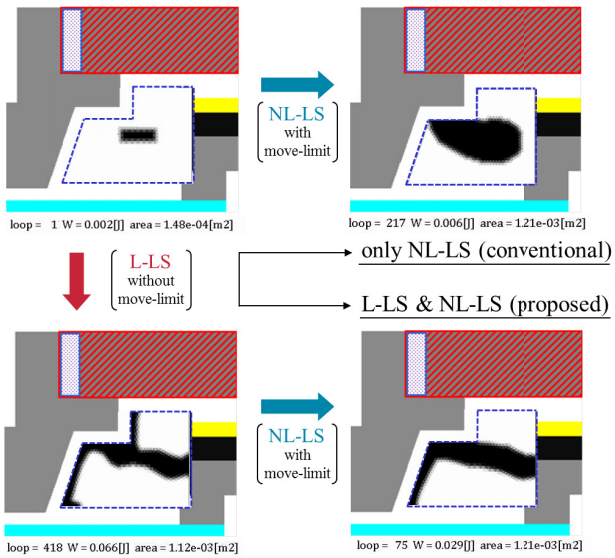

Loop, W, and area in the figure are the iteration number, the objective function value, and the area of the shape respectively.

Fig. 10. Optimization results by only NL-LS and combined L-LS & NL-LS, with an initial shape of a horizontally long rectangle

4.2 2D Level-set Method Results As described before, we propose an ingenious technique of combined nonlinear level-set method (NL-LS) with linear level-set method (L-LS), i.e., we carry out an initial conceptual design by L-LS to derive the initial shape of NL-LS. Furthermore, we also propose move-limit strategy detailed in 3.2.5 to prevent the configuration from unfavorable deformation by the operation of area constraint. In this subsection, we confirm the validity of our proposals by showing results of the conventional and proposed methods.

Figure 9 and Fig. 10 show the comparison of results between only NL-LS (conventional) and combined L-LS and NL-LS (proposed), with initial shapes of a square and a horizontally long rectangle. Figure 11 shows the objective function values of results in Fig. 9 and Fig. 10. The shapes in Fig. 9 and Fig. 10 are qualitatively valid because the magnetic materials are distributed near the target area Ω_t and they have thick shapes in NL-LS while satisfying the area constraint condition. Since thin shapes are permissible and the area constraint is always inactive in L-LS, it does not enter the move-limit scheme. Figure 9, Fig. 10, and Fig. 11 indicate that the proposed method has the better results than the conventional one regardless of the initial shape because the L-LS in the proposed method is able to derive the proper initial shape of NL-LS. Especially, when inputting a horizontally long rectangle, whereas the optimal shape by the conventional method (in upper right of Fig. 10) does not reach the existing silicon steel near the exciting coil on account of the area constraint, the optimal shape by the proposed method (in lower right of Fig. 10) is able to reach it because of the initial conceptual design by L-LS.

To verify the move-limit strategy, we compare Fig. 9 to Fig. 12 which shows the results without move-limit, by only NL-LS and combined L-LS and NL-LS, with an initial shape of a square. In comparison with Fig. 9, the shapes in Fig. 12 are less feasible due to excess correction of the configuration by area constraint operation. Similarly, the results from an initial shape of a horizontally long rectangle display this same tendency.

4.3 Decision of Final 3D Designs We obtain the two 2D optimal shapes by the combined L-LS and NL-LS with move-limit, in the lower right of Fig. 9 and Fig. 10, which indicate the optimal magnetic circuit. Next, we convert the two shapes into straight line configurations to facilitate the manufacture while maintaining the magnetic circuit, as shown in Fig. 13. We confirm that this conversion causes no performance deterioration by analyzing 3D designs, of the rotated the cross-sections, with 3D coupled magnetic-thermal FEM.

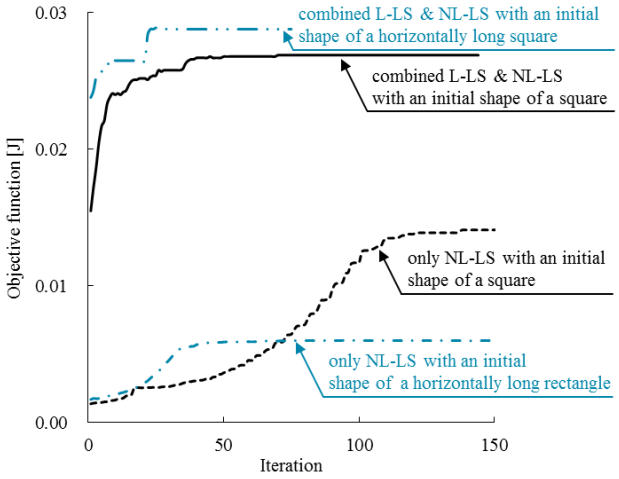

Fig. 11. Comparison of the objective function values between only NL-LS and combined L-LS & NL-LS

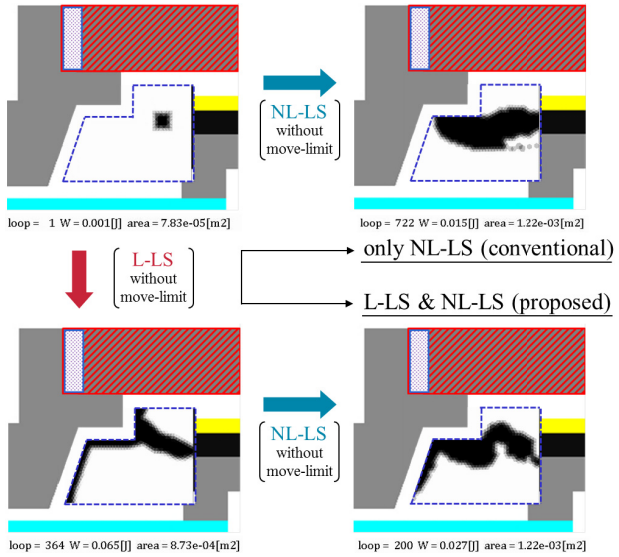

Loop, W, and area in the figure are the iteration number, the objective function value, and the area of the shape respectively.

Fig. 12. Optimization results without move-limit, by only NL-LS and combined L-LS & NL-LS, with an initial shape of a square

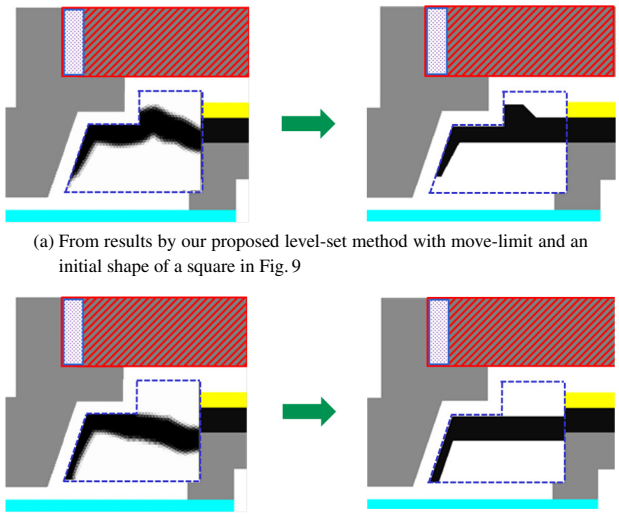

(a) From results by our proposed level-set method with move-limit and an initial shape of a square in Fig. 9

(b) From results by our proposed level-set method with move-limit and an initial shape of a horizontally long rectangle in Fig. 9

Fig. 13. Conversion into straight line configurations to improve the manufacturability

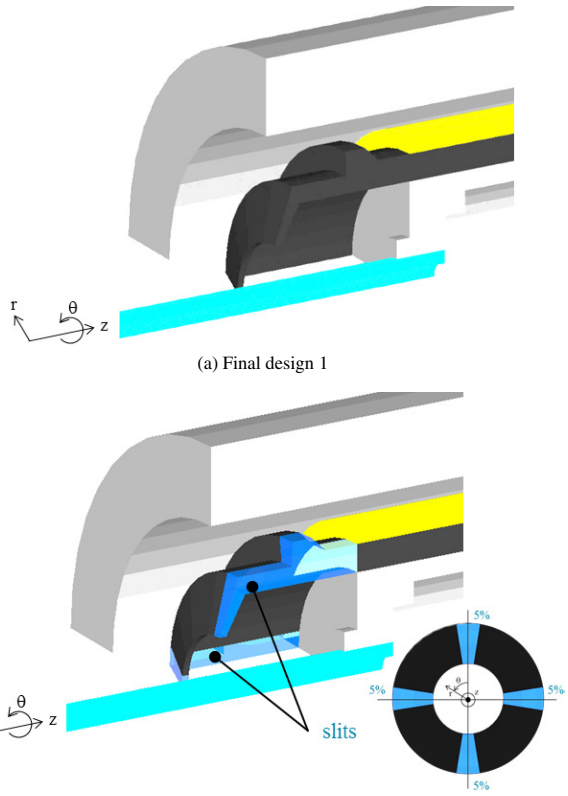

(a) Final design 1

(b) Final design 2 with slits

Fig. 14. Final designs of our proposed design optimization (rθ:1/4, z:1/2)

Although we create two 3D designs from the converted cross-sections in Figs. 13(a) and (b), we choose the 3D design from Fig. 13(a) because this design has better heating performance according to 3D FEM. This chosen 3D design is called final design 1 and shown in Fig. 14(a). Here, the volume of the final design 1 is 1.26 times as great as the volume of the current design as shown in Table 2 because the material is farther from the axis of rotation. Hence, we insert 20% slits, or air gaps, in the tip of the primary core which are uniformly arranged into four locations in the circumference direction so that the volume is the same as the current design. From the viewpoints of both magnetic and thermal circuits, it is considered that the slits arrangement hardly affects the heating performance in consideration with the fact that the width of slit is small and heating part rotates in actual use. With the above assumption, in this paper, we independently perform the cross-section optimization and slits arrangement. This design is called final design 2 and is shown in Fig. 14(b). The effectiveness of final design 2 is demonstrated with computational results of heating performance in the later section 4.4.

4.4 Heating Performance of the Final Designs Evaluated by 3D Coupled Magnetic-Thermal FEM Finally, we calculate the heating performance of the current design, final design 1, and final design 2 by 3D coupled magnetic-thermal analysis with magnetic nonlinearity. Since the performance of the heating speed has the same tendency across the surface of the heating part, we only show the surface

Table 2. Volume values of current design and final design 1, 2

	Current design	Final design 1	Final design 2 with slit
Volume [m^3]	4.426×10^{-4} (1.00)	5.556×10^{-4} (1.26)	4.444×10^{-4} (1.00)

The value in parentheses is the proportion of the volume of each design to that of the current design.

Table 3. Surface temperature of the heating part at steady state

	Current design	Final design 1	Final design 2 with slit
Edge [°C]	308.7	321.5	320.3
Center [°C]	507.7	513.2	512.2
Edge/Center	0.6080	0.6266	0.6253

temperature at the edge of the heating part T_{edge} and at the center T_{center} as pointed in Fig. 1, which are the maximum and minimum points respectively. Temperature uniformity on the surface of the heating part is assessed as the ratio between T_{edge} and T_{center} as calculated in (25). The complete uniformity means 1.0.

$$\textit{Surface temperature uniformity} = T_{edge}/T_{center} \quad \cdots\cdots\cdots\cdots\cdots\cdots (25)$$

The transient values of these aspects of heating performance are shown in Fig. 15 and the values at the steady state are shown in Table 3. Figures 15(a) (b) show that the final 3D designs improve the heating speed on the surface of the heating part in spite of optimizing the primary core tip which is limited region depicted as the design domain in Fig. 1. Since we modify the shape of the primary core tip, the improvement at the edge is greater than that at the center. Because of the improvement at the edge, the temperature uniformity is ameliorated as shown in Fig. 15(c). Furthermore, final design 2 with slit structure, which has the same volume as the standard, hardly deteriorates the heating performance in comparison with final design 1. Therefore, the final design of this paper successfully improves both heating speed and temperature uniformity on the surface of the heating part under the same input AC current and material volume, which demonstrates the validity of our proposed design optimization.

5. Conclusions

In this paper, we propose a novel practical design optimization of primary core in induction heating roll by level-set method. The new ideas can be summarized as follows:

1) We effectively combine 2D magnetostatic level-set method and 3D coupled magnetic-thermal FEM from the viewpoint of the computational cost.
2) In level-set method, we propose an ingenious approach with the initial conceptual design by linear level-set method before nonlinear level-set method. Furthermore, we also propose the move-limit strategy for preventing unfavorable deformation during the operation for area constraint.
3) The optimal shape by our proposed 2D level-set method is converted into a straight line cross-sectional configuration to facilitate manufacture. When creating the 3D shape by rotating the cross-section, we propose a novel structure with slits, or air gaps, in the tip of the primary core in order to reduce the volume while retaining the heating performance.
4) As a result of 3D coupled magnetic-thermal analysis

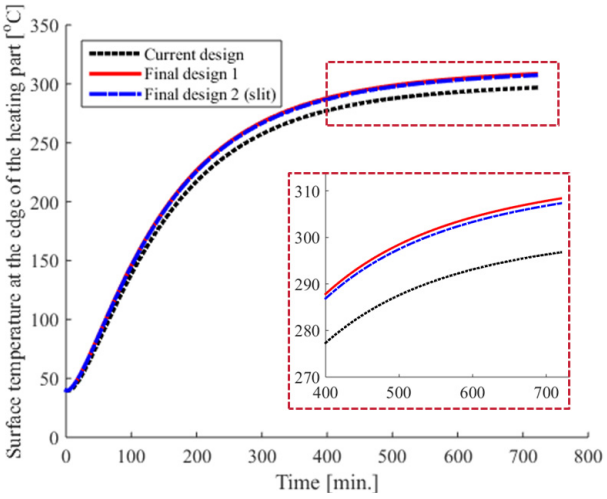

(a) Transient surface temperature at the edge of the heating part

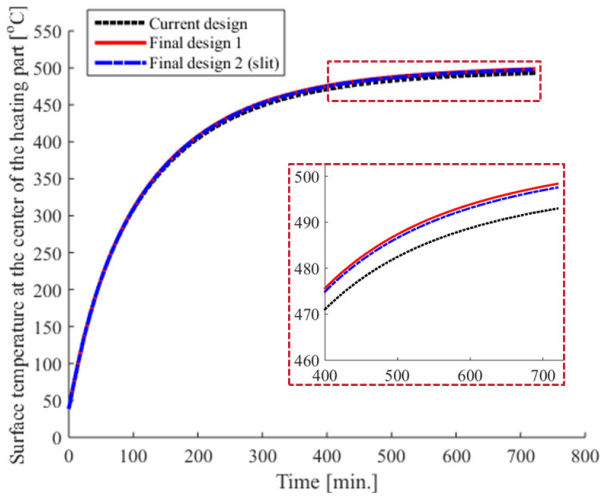

(b) Transient surface temperature at the center of the heating part

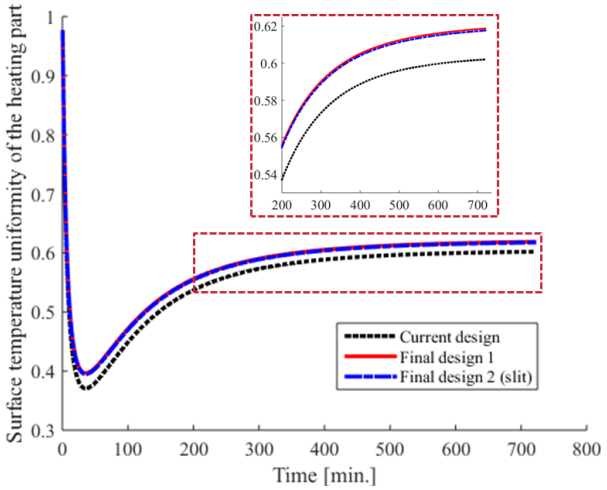

(c) Transient surface temperature uniformity in the heating part

Fig. 15. Comparison of heating performance between the current design and the final design 1, 2

with magnetic nonlinearity, the final 3D design successfully improves heating speed and temperature uniformity on the surface of the heating part under the same conditions of input AC current and material volume.

References

(1) S.M. Jang, S.K. Cho, S.H. Lee, H.W. Cho, and H.C. Park: "Therrmal analysis of induction heating roll with heat pipes", *IEEE Trans. Magn.*, Vol.39, No.5, pp.3244–3246 (2003)

(2) M. Kranjc, A. Županič, T. Jarm, and D. Miklavčič: "Optimization of induction heating using numerical modeling and genetic algorithm", 2009 35th Annual Conf. of IEEE Industrial Electronics, Porto, 2009, pp.2104–2108 (2009)

(3) I. Lope, J. Acero, and C. Carretero: "Analysis and Optimization of the Efficiency of Induction Heating Applications With Litz-Wire Planar and Solenoidal Coils", *IEEE Trans. Power Electron.*, Vol.31, No.7, pp.5089–5101 (2016)

(4) S.I. Park and S. Min: "Design of Magnetic Actuator With Nonlinear Ferromagnetic Materials Using Level-Set Based Topology Optimization", *IEEE Trans. Magn.*, Vol.46, No.2, pp.618–621 (2010)

(5) Y. Okamoto, S. Wakao, and S. Sato: "Topology Optimization Based on Regularized Level-Set Function for Solving 3-D Nonlinear Magnetic Field System With Spatial Symmetric Condition", *IEEE Trans. Magn.*, Vol.52, No.3, pp.1–4 (2016)

(6) Y. Okamoto, H. Masuda, Y. Kanda, R. Hoshino, and S. Wakao: "Convergence Acceleration of Topology Optimization Based on Constrained Level Set Function Using Method of Moving Asymptotes in 3-D Nonlinear Magnetic Field System", *IEEE Trans. Magn.*, No.99 (2017)

(7) Q. Xia, M.Y. Wang, and T. Shi: "A move limit strategy for level set based structural optimization", Engineering Optimization, Vol.45, pp.1061–1072 (2012)

(8) T. Mifune, Y. Takahashi, and K. Fujiwara: "Complex-valued formulation of nonlinear time-harmonic magnetic field analysis and new Krylov-like solvers", Proc. 2016 IEEE Conf. on Electromagnetic Field Computation (CEFC), Miami, FL, 2016, pp.1–1 (2016)

Kazuki Hirono (Student Member) was born in Tokyo, Japan in 1992. He received a B.S. degree in electrical engineering and bioscience from Waseda University, Tokyo, Japan in 2015, and is presently a candidate for a M.S. degree in electrical engineering and bioscience. His research interests include design optimization of induction heating machines and optimization methods.

Reona Hoshino (Student Member) was born in Tokyo, Japan in 1992. He received a B.S. degree in electrical engineering and bioscience from Waseda University, Tokyo, Japan in 2015, and is presently a candidate for a M.S. degree in electrical engineering and bioscience. His research interests include optimization methods for electrical machinery.

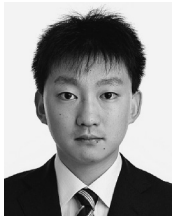

Tsuyoshi Kamiya (Student Member) was born in Tokyo, Japan in 1994. He received a B.S. degree in electrical engineering and bioscience from Waseda University, Tokyo, Japan in 2016, and is presently a candidate for a M.S. degree in electrical engineering and bioscience. His research interests include optimization methods for electrical machinery.

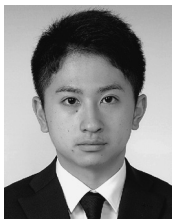

Shinji Wakao (Member) was born in Fukuoka, Japan in 1965. He received B.S., M.S., and Ph.D. degrees in 1989, 1991 and 1993, respectively, from Waseda University, Tokyo, Japan. He became a Professor in the Department of Electrical Engineering and Bioscience in 2006, and since 2016, he has been the the Dean of School of Advanced Science and Engineering, Waseda University. He is an executive board member of Japan Solar Energy Society, a member of an electric power safety commission in the Ministry of Economy, Trade and Industry, Japan, etc. His research interests are electromagnetic field computation, photovoltaic power generation system, and design optimization of electric machines.

Yoshifumi Okamoto (Senior Member) received Ph.D. degree in 2005 from Okayama University, Japan. After that, engaged in postdoctoral researcher at RIKEN and so on, he became an associate professor in the department of electrical and electronic engineering in 2015. His research interests are advanced methodology for electromagnetic field computation, topology optimization method of electrical machine, and parallel computation. He is a member of IEEE, the International Compumag Society, and the Japan Society for Computational Engineering and Science.

Woojin Jeon (Non-member) was born in Korea in 1967. He received B.S. degree in electrical engineering from Konkuk University, Seoul, Korea in 1991, and M.S. and Ph.D. degrees in electrical engineering in 1995 and 1998, respectively, from Waseda University, Tokyo, Japan. He was a scholarship recipient of the Japanese ministry of education, and becomes CEO of DONGWONROLL Co., Ltd. since 2006.